JOURNAL OF CATALYSIS 154, 276–287 (1995)

Alumina-Supported Pt–Rh Catalysts

II. Kinetic Characterization and Synergistic Effects

Rollin E. Lakis,[1] Yeping Cai,* Harvey G. Stenger, Jr.,[2,*] and Charles E. Lyman

*Materials Science and Engineering Department, and *Chemical Engineering Department, Lehigh University, Bethlehem, Pennsylvania 18015*

Received March 17, 1994; revised November 2, 1994

Analytical electron microscopy was used in the preceding paper to determine the composition distribution of individual catalytically active particles on several supported Pt–Rh bimetallic catalysts. The kinetic performance of these catalysts for the reduction of NO with H_2 and the reduction of NO with CO between 25 and 300°C is presented here. The performance of one catalyst that contained alloy particles with compositions centered at approximately 10 wt% Pt and 90 wt% Pt was intermediate to that observed for Pt and Rh monometallic catalysts. Additional catalysts were prepared to separately test the kinetic performance of Pt-rich and Rh-rich alloy particles. One catalyst that was prepared at a 95/5 weight ratio of Pt to Rh contained Pt-rich alloy particles in the composition range of 80 wt% Pt–100 wt% Pt. Another catalyst was prepared at a 17/83 weight ratio of Pt to Rh and contained mostly Rh-rich alloy particles in the composition range of 70 wt% Rh–100 wt% Rh. For both the NO–H_2 and NO–CO reactions, the 95/5 catalyst displayed an activity greater than that expected from the sum of the alloy components. It is therefore concluded that for the Pt-rich alloy particles of the 95/5 catalyst, a synergistic effect due to particle alloying is present. The kinetic performance of the Rh-rich particles in the 17/83 catalyst was less favorable, and less than that expected from the sum of the alloy components for the NO–CO reaction. © 1995 Academic Press, Inc.

INTRODUCTION

The presence or absence of synergistic performance effects due to particle alloying in the Pt–Rh system has been debated in the literature for a number of years. Convincing evidence that supports the presence of reaction synergism for CO oxidation was presented by Oh and Carpenter in 1986 (1). These authors showed that the CO oxidation activity of a certain Pt–Rh alloy catalyst was substantially higher than the activity of an equivalent physical mixture. Reaction synergism was measured as a function of bulk composition, and maximum synergism was observed for the catalyst with the highest relative Pt content (90/10) in their study. Their catalysts, which displayed reaction synergism, were prepared by sequential impregnation. Rhodium was impregnated first and calcined in air at 300°C, then the Pt was impregnated using acetone (2), and the catalyst was calcined at 500°C for 4 h. Also in their study, coimpregnated catalysts calcined at 500°C with an average metal composition of 60 wt% Pt, did not show reaction synergism. They did not measure particle compositions or present any detailed characterizations. Tzou *et al.* (3) claim synergistic effects for CO oxidation and the NO–CO reaction for Pt–Rh alloys prepared on NaY zeolite. The reaction data in this case were presented as T_{50} (temperature at which 50% conversion was observed) and not on a surface-site basis making direct kinetic comparisons difficult.

Nieuwenhuys and his research group have published data which do not support the presence of alloy synergism (4, 5). These workers claim that their Pt–Rh alloys did not display a synergistic activity effect due to particle alloying for either CO oxidation or the NO–CO reaction. For these studies, the precursors were coimpregnated in silica and reduced at about 400°C. They observed gradually changing performance characteristics for Pt–Rh alloys between the limits defined by the performance of monometallic Pt and Rh.

These conflicting results highlight the controversy concerning the presence of a synergistic catalytic effect due to particle alloying. A graphical definition of reaction synergism for a hypothetical catalytic reaction and alloy system is presented in Fig. 1. For this system Metal A displays a much greater activity than Metal B, and for simplicity, the reaction rate contribution of Metal B can be ignored. If an alloy catalyst is prepared which contains an equal number of active Metal A sites and Metal B sites, then the reaction rate constants for this catalyst are expected to be one half those observed for Metal A alone (labeled average performance in Fig. 1). Because the reaction rate constants for Metal A and Metal B have not changed, and only one half of the alloy catalyst sites are

[1] Present address: University of Pennsylvania, Philadelphia, PA 19104.

[2] To whom correspondence should be addressed.

0021-9517/95 $12.00

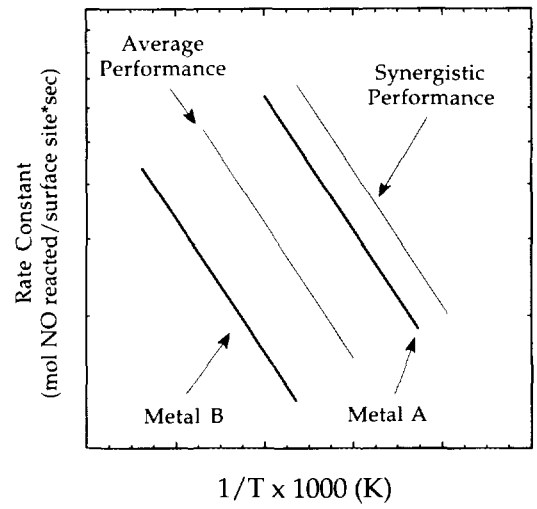

FIG. 1. A hypothetical model of the reaction rate constants of an alloy catalyst which depicts the presence and absence of a synergistic activity effect due to particle alloying.

Metal A, on a per-site basis the alloy catalyst is half as active as Metal A. Fundamental to this prediction is the assumption that the two metals are noninteracting, and behave independently even though they are alloyed. Another possibility is that the A–B alloy performs better than Metal A alone. This performance is termed synergistic (labeled synergistic performance in Fig. 1) because the addition of Metal B, which alone does not contribute greatly to the reaction, has improved the performance of Metal A. This is different from catalytic promotion in that if Metal B were a promoter metal, it would have zero activity. It is also possible that Metal B could interfere with the reaction over Metal A, and decrease the anticipated performance of the alloy to below what is expected from the 50% of sites which are Metal A. Synergistic alloying effects are not limited to catalytic activity, synergistic improvements in reaction selectivity and durability can be equally important.

In the previous paper (6), it was established that when Pt and Rh are prepared in the same support material they form alloy particles. The presence or absence of a synergistic effect due to particle alloying is therefore an important unresolved issue in Pt–Rh alloy catalyst research. This investigation will address the synergism issue and focus upon relating the composition and microstructure of individual catalytically active particles to their kinetic performance. Analytical electron microscopy (AEM), when coupled with traditional gas adsorption and reaction studies, enables the characterization of highly dispersed bimetallic systems. With the use of AEM, the effects of particle chemistry and microstructure on the catalytic properties of activity and selectivity may be determined.

In the present study, we report the steady-state reaction rates for NO reduction with H_2 and CO from 50 to 300°C, including reaction selectivity data for the Pt–Rh alloy catalysts that were characterized in the previous paper. The performance of these alloy catalysts is compared to that of monometallic catalysts which contain only Pt or Rh. The objectives of this investigation are to determine whether synergism in activity and/or selectivity can be detected in alloy catalysts and whether the kinetic properties of the alloy catalysts can be related to the compositions of the individual particles which were determined in the previous paper (6).

EXPERIMENTAL

Catalyst Preparation

Nine catalysts were prepared for this investigation, two monometallic catalyst which contained Pt or Rh and seven Pt–Rh alloy catalysts which were prepared using different impregnation techniques. The details of the preparation procedures for these catalysts were previously presented (6) and are summarized in Table 1.

Catalytic Testing

Figure 2 shows the catalytic testing apparatus built for this investigation. It was used to determine the activity and selectivity of the catalysts for the NO–H_2 and NO–CO reactions. The gases used in the reactor (MG Industries, certified mixtures), 0.5% nitric oxide in helium, 1% hydrogen in helium, 1% carbon monoxide in helium, 99.999% helium, and 99.99% hydrogen are metered into the reactor system through separate flow meters (Brooks, Sho-Rate). A back pressure regulator is located down stream of the flow meters to maintain a constant pressure in each flowmeter, and allow a flow rate calibration for each flowmeter and gas combination which is independent of the total flow rate. Two fused silica reactor tubes, 10 mm i.d. and 40 cm long are supported inside a

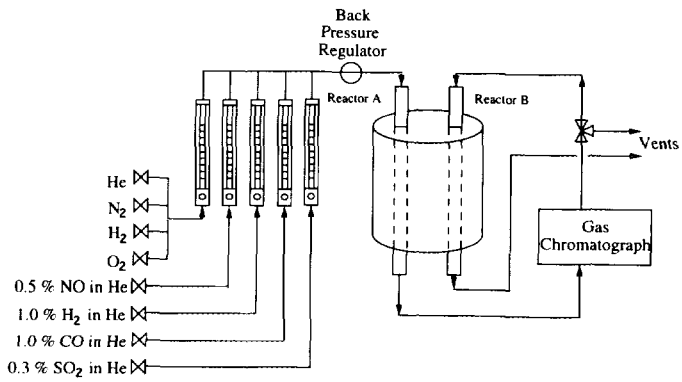

FIG. 2. Schematic diagram of catalytic reactor system constructed for this investigation.

TABLE 1

Summary of the Microstructural Characteristics of Each Catalyst

Catalyst	Bulk composition	Preparation procedure	AEM particle composition distribution	XPS	Dispersion (%)
Pt	0.53% Pt	Impreg, air-dry, reduce 300°C 12 h	—	—	61
Rh	0.40% Rh	Impreg, air-dry, reduce 300°C 12h	—	—	41
60/40	0.61% Pt 0.40% Rh	Pt impreg, air-dry, calcined 500°C in air 3 h, Rh impreg, air dry, reduce 300°C 12 h	Bimodal 12.5% Pt 92.5% Pt	8% Pt 92% Rh	51
60/40A	0.61% Pt 0.40% Rh	Pt impreg, air-dry, calcined 500°C in air 3 h, Rh impreg, air dry, reduce 700°C 72 h	Broad distribution 65% Pt	54% Pt 46% Rh	44
95/5	1.42% Pt 0.078% Rh	Pt impreg, air-dry, calcined 500°C in air 3 h, Rh impreg, air dry, reduce 300°C 12 h	Unimodal 97.5% Pt	—	32
17/83	0.21% Pt 1.02% Rh	Pt impreg, air-dry, calcined 500°C in air 3 h, Rh impreg, air dry, reduce 300°C 12 h	Unimodal 17.5% Pt	—	80
75/25	1.18% Pt 0.39% Rh	Rh impreg, air-dry, calcined 500°C in air, pt impreg, air dry, reduce 300°C 12 h	Unimodal 97.5% Pt	Rh present in mixed oxidation states	55
72/28-ox	0.73% Pt 0.29% Rh	Coimpreg, calcined 500°C 3 h, reduced 300°C 12 h	Bimodal 2.5%, 97.5% Pt	—	—
72/28-red	0.73% Pt 0.29% Rh	Coimpreg, reduced 300°C 12 h	Bimodal 2.5%, 87.5% Pt	—	—

6.35-cm bore tube furnace by an insert made of machineable ceramic to accommodate the reactor tubes. The catalyst powder is supported in the middle of the reactor tubes by a fused silica frit. The temperature of the catalyst is measured by a K-type thermocouple inserted axially down the primary reactor tube and placed in the catalyst bed. Inlet and outlet gases are analyzed using a Carle 111H dual column gas chromatograph (GC) with a 1-cc sample loop utilizing a 7-ft Haysep D column for the analysis of N_2O and CO_2. A 15-ft Carboxen 1000 column provides analytic separation for O_2, N_2, NO, and CO. A single injection provides a complete analysis of the gases of interest in approximately 20 min. The GC response was calibrated for NO, CO, N_2, N_2O, and H_2 using gas mixtures of known composition. During NO–CO analysis, the nitrogen material balance typically closed to within 10%. Downstream of the reactor outlet and the GC, the reaction gases may be vented, or diverted through the second reactor tube which may contain additional catalyst. The purpose of the second reactor is to expose additional catalyst material to a reaction environment similar to the primary reactor. A sample may be removed for analysis from the secondary reactor when the catalytic performance and reaction history of the primary reactor is known, without significantly disturbing the primary reactor. The furnace temperature is monitored by a K-type thermocouple placed between the ceramic insert and the furnace wall. Temperature control is performed by a Zenith Z-158 personal computer running Control EG software (Quinn-Curtis).

Steady-state reaction rates were measured using 1 : 1 molar ratios of NO–H_2 and NO–CO mixtures from room temperature to 300°C. The NO reaction rate was determined from the difference between inlet and outlet concentrations of NO. Typically, 0.50 g of catalyst powder was placed in the primary reactor tube. The total flow rate was maintained at 128 std cc/min for a space velocity of 20,000 h^{-1} (volume of gas/volume of catalyst per hour), and the nominal inlet concentrations of NO, H_2, and CO were 3500 ppm. After GC injections, the temperature was changed and allowed to equilibrate at the next set point during the 20 min required for the GC analysis of the reaction products. Each catalyst was loaded into the primary reactor, reduced at 300°C in flowing H_2 for 12 h,

and allowed to cool in the reactor to room temperature. Following reduction, each catalyst was tested twice from room temperature to 300°C using the NO–H_2 reaction mixture. Next, the NO–CO reaction was run twice, and finally, the NO–H_2 reaction was run a third time.

It was observed that when testing Pt catalysts (including alloy catalysts), after the first two NO–H_2 temperature-conversion runs were performed, the first NO–CO reaction proceeded more rapidly than the second. After the second reaction no changes were observed. After NO–CO testing was complete, and additional NO–H_2 runs were performed, the original activity was nearly recovered. This type of activation behavior has been observed elsewhere in CO oxidation studies (7). This change in activity was not observed for the Rh monometallic catalyst.

KINETIC THEORY

Overall reactions for the reaction of NO by H_2 include:

$$NO + H_2 \rightarrow 1/2\,N_2 + H_2O \quad [1]$$

$$2\,NO + H_2 \rightarrow N_2O + H_2O \quad [2]$$

$$NO + 5/2\,H_2 \rightarrow NH_3 + H_2O. \quad [3]$$

Because the reduction of NO to N_2 is the most desirable reaction, the selectivity of these catalysts is presented as the ratio of exiting N_2 concentration to the N_2O concentration

$$\text{Selectivity} = \frac{C_{N_2}}{C_{N_2O}}, \quad [4]$$

where C_{N_2} and C_{N_2O} represent the respective gas concentrations at the reactor outlet. The NH_3 concentration was not measured independently, but since no other nitrogen containing species was formed, the NH_3 concentration may be calculated by closing the nitrogen material balance.

To evaluate the catalytic activity effects of particle alloying, the steady-state reaction rate constants of pure Pt and Rh will be compared with the rate constants of the alloy catalysts.

The NO–H_2 reaction was modeled using Langmuir–Hinshelwood kinetics for a bimolecular reaction of adsorbed NO with a disassociatively adsorbed H atom (8). The surface reaction was assumed to be the rate-limiting step, and product adsorption was assumed to be negligible. The complete expression is

$$\nu_{NO} = \frac{k_{SR} K_{NO} P_{NO} K_{H_2}^{0.5} P_{H_2}^{0.5}}{(1 + K_{NO} P_{NO} + K_{H_2}^{0.5} P_{H_2}^{0.5})^2}, \quad [5]$$

where ν_{NO} represents turnover frequency, k_{SR} is the surface reaction rate constant, K_i represents the equilibrium adsorption rate constant for the respective species, and P_i is the partial pressure of the respective gas. If the surface coverage of NO is assumed to be much greater than H_2, and if NO nearly saturates the surface, Eq. [5] reduces to

$$\nu_{NO} = \frac{k_{SR} K_{H_2}^{0.5} P_{H_2}^{0.5}}{K_{NO} P_{NO}}. \quad [6]$$

The apparent reaction rate constant ($k_{NO\text{-}H_2}$) can defined in the following manner:

$$k_{NO\text{-}H_2} = \frac{k_{SR} K_{H_2}^{0.5}}{K_{NO}}. \quad [7]$$

The reduced Langmuir–Hinshelwood model (presented below) was related to the measurements made in this study through the right-hand side of the equation

$$\nu_{NO} = k_{NO\text{-}H_2} \frac{\bar{P}_{H_2}^{0.5}}{\bar{P}_{NO}} = \frac{\Delta C_{NO} \dot{V}}{S^*_{Pt+Rh}} \quad [8]$$

where ν represents turnover frequency (mol NO reacted/surface site · second), $k_{NO\text{-}H_2}$ is the apparent reaction rate constant (mol NO reacted · $kPa^{0.5}$/surface site · second), $\bar{P}$ is the average partial pressure (kPa) of the respective gas which is set equal to the linear average of P_{in} and P_{out}, ΔC_{NO} is the change in NO concentration, $\dot{V}$ is the space velocity, and S^*_{Pt+Rh} is the total number of metal surface sites calculated from CO or H_2 chemisorption (6). This reaction rate model was shown to adequately represent this reaction by previous investigators (9, 10).

Primary reactions for the reduction of NO by CO include

$$NO + CO \rightarrow 1/2\,N_2 + CO_2 \quad [9]$$

$$2\,NO + CO \rightarrow N_2O + CO_2. \quad [10]$$

Reaction [9], which leads to the formation of N_2, is the most desirable reaction. The NO–CO reaction selectivity is calculated in the same manner as the NO–H_2 selectivity.

It appears from other studies that in the NO–CO reaction, the concentration dependence on NO and CO is quite different between Pt and Rh catalysts. Over silica supported Pt catalysts, the reaction rate was reported to be first order in NO and negative second order in CO (13). In another study the pressure dependence on CO over polycrystalline Pt was shown to vary with temperature (21). Over the Rh(100) single-crystal structure, Hendershot and Hansen (22) observed the CO kinetic order

varied continuously from +1 to −1 and the NO kinetic order from +1.5 to −1. Bell's research group (23), on the other hand, investigated the NO–CO reaction over silica-supported rhodium catalysts. They reported that the kinetic order for NO reduction was slightly positive in CO but slightly negative in NO. A closer investigation of their work reveals that both NO and CO can be assumed to be zero order in the reaction. The rate expression for the NO–CO reaction is thus presented

$$\nu_{NO} = k_{NO\text{-}CO}\bar{P}^0_{NO}\bar{P}^0_{CO} = \frac{\Delta C_{NO}\dot{V}}{S^*_{Pt+Rh}}, \qquad [11]$$

where ν represents turnover frequency (mol NO reacted/surface site · second), $k_{NO\text{-}CO}$ is the apparent reaction rate constant (mol NO reacted/surface site · second), $\bar{P}$ is the average partial pressure (kPa) of the respective gas which is set equal to the linear average of P_{in} and P_{out}, ΔC_{NO} is the change in NO concentration, $\dot{V}$ is the space velocity, and S^*_{Pt+Rh} is the total number of metal surface sites calculated from CO or H_2 chemisorption (6). The above Eq. [11] should be also valid for a Pt–Rh alloy. As it will be shown in Results, Rh is orders of magnitude greater in activity than Pt. Thus, a rate expression for an alloy can be approximately represented by Eq. [11].

To avoid the effects of secondary reactions, and permit the assumption of a differential reactor, only data with NO conversions of less than 50% were evaluated.

RESULTS

NO Reduction Activity

Nitric oxide conversion versus temperature data for the monometallic catalysts are presented in Fig. 3. It is important to note that for both the NO–H_2 and the NO–CO reaction the reaction rates for Rh are similar, but the Pt reaction rate changes dramatically. For Pt, the temperature of 50% conversion (T_{50}) of NO for the NO–CO reaction is 230°C higher than the T_{50} for the identical material evaluated using the NO–H_2 reaction. In contrast, the Rh NO–CO T_{50} is only 10°C higher than the NO–H_2 T_{50}. In the case of Pt, the large difference in T_{50} for the H_2 and CO reactions may be indicative of a change in the rate-limiting reaction step and/or surface concentrations of reacting species. Regardless of the mechanism, CO was observed to severely reduce the reduction rate of NO over Pt. In the case of Rh, the magnitude of the reduction in reaction rate is considerably smaller and hardly observable.

The NO reduction rate constants for the NO–H_2 reaction are presented in Fig. 4. At a given temperature, the rate constants for Pt are approximately three orders of magnitude greater than those for Rh. The observed

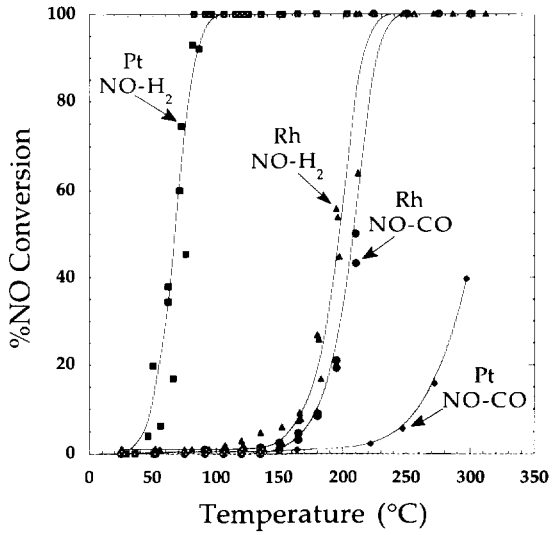

FIG. 3. Comparison of NO conversion curves of the Pt and Rh monometallic catalysts for both probe reactions. Symbols: squares, Pt NO–H_2; triangles, Rh NO–H_2; circles, Rh NO–CO; diamonds, Pt NO–CO.

NO–H_2 reaction rate constants of the 60/40 and 60/40A alloy catalysts are similar (the 60/40A catalyst was slightly higher) and are between those of the monometallic catalysts. The NO reduction activity of the 17/83 catalyst is slightly greater than that of the Rh monometallic catalyst. A very different result was obtained for the 95/5 catalyst. At a given temperature, the rate constants for the reduction of NO (NO–H_2) over the 95/5 catalyst were approxi-

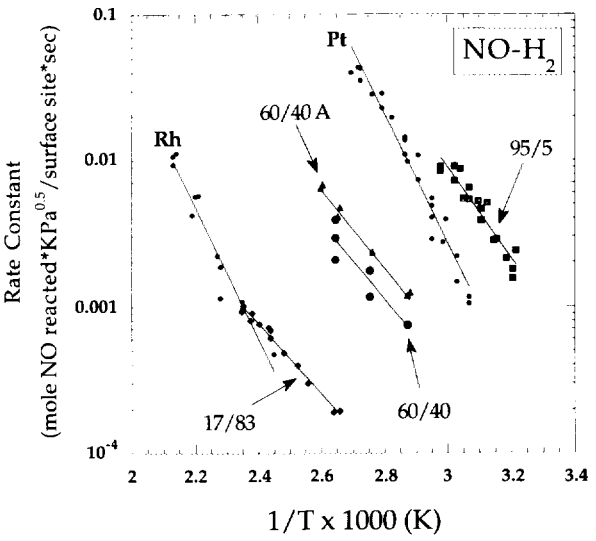

FIG. 4. Plot of log reaction rate constants of the monometallic catalysts, 60/40, 60/40A, 17/83, and 95/5 catalysts versus inverse temperature for the NO–H_2 reaction. Symbols: squares, 95/5; circles, 60/40; triangles, 60/40A; diamonds, 17/83.

mately five times greater than those of the Pt monometallic catalyst.

The NO–H_2 reaction rate constants of the 75/25 catalyst are presented in Fig. 5. These results are compared with several of the reaction-rate curves from Fig. 4. The 75/25 catalyst displayed reaction rate constants greater than monometallic Pt, but less than the 95/5 catalyst which was the most active catalyst for the NO–H_2 reaction. This phenomenon is observed to hold regardless of the form of the kinetic rate expression used.

Both 72/28 coimpregnated catalysts performed similarly for the NO–H_2 reaction, and these results are also presented in Fig. 5. The metallic dispersion of the coimpregnated catalysts was not measured, therefore a range of performance is indicated for actual dispersions between 30 and 70% (dotted lines). The observed NO–H_2 reaction rate constants for these catalysts are slightly less than those observed for the Pt monometallic catalyst (lower slope), but are significantly greater than those observed for the 60/40 catalyst.

The apparent activation energies for this reaction have been calculated from the slope of the lines in the Arrhenius-type plots and the values for each of the catalysts are presented in Table 2. In general, the calculated apparent activation energies of the alloy catalysts are substantially less than those observed for the Pt and Rh monometallic catalysts.

For the NO–CO reaction the reaction-rate constants for Rh are two orders of magnitude greater than those for Pt (Fig. 6). This is opposite from the observation made for the NO–H_2 reaction, where Pt was much more reactive than Rh. The 60/40 and 60/40A catalysts displayed similar

TABLE 2

Summary of Observed Apparent Activation Energy and Preexponential Factor for the Apparent Reaction Rate Constants: $k_a = A \exp(-E_a/RT)$

Catalyst	NO–H_2 A^a	NO–H_2 E_a (kJ/mol)	NO–CO A^b	NO–CO E_a (kJ/mol)
Pt	6.08 E10	85.2	5.63 E6	91.0
Rh	3.50 E7	85.8	3.52 E6	78.7
60/40	5.16 E4	51.0	1.27 E11	121
60/40A	1.86 E4	49.4	7.07 E10	121
17/83	4.52 E2	46.1	8.41 E11	133
95/5	1.83 E7	59.4	1.06 E5	64.3

[a] (Mol NO reacted*$KPa^{0.5}$/surface site*s.)
[b] (Mol NO reacted/surface site*s.)

NO reduction rate constants for the NO–CO reaction (the 60/40A catalyst was slightly higher), which were between those observed for the monometallic catalysts, but closer to the values of the Rh monometallic catalyst. The performance of the 17/83 catalyst for the NO–CO reaction was between that of the Pt and Rh monometallic catalysts. However, the 95/5 catalyst displayed rate constants approximately equal to those of the Rh monometallic catalyst. This is a surprising result because Rh is more active than Pt for NO reduction by CO, and the 95/5 alloy catalyst which contains the least Rh displays the most Rh-like behavior. The similarity in activity between the Rh and 95/5 catalysts is also revealed in the NO temperature versus conversion data (not shown).

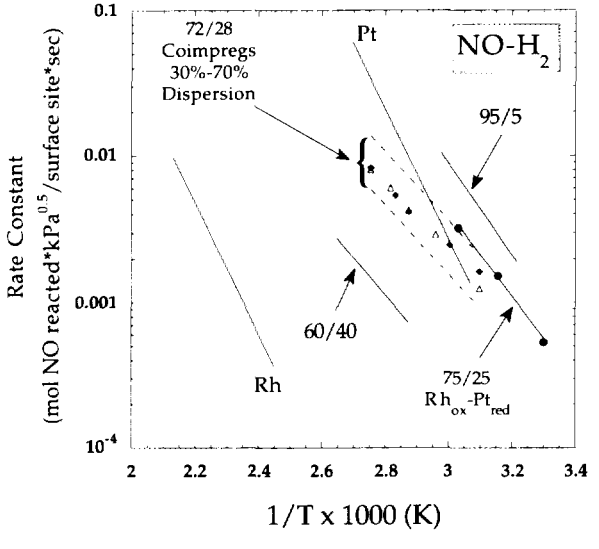

FIG. 5. Plot of log reaction rate constants of the 72/28 coimpregnated catalysts, and the 75/25 Rh_{ox}–Pt_{red} versus inverse temperature for the NO–H_2 reaction. Additional data from Fig. 4 for reference. Symbols: diamonds, 72/28 ox; open triangles, 72/28 red; circles, 75/25 Rh_{ox}–Pt_{red}.

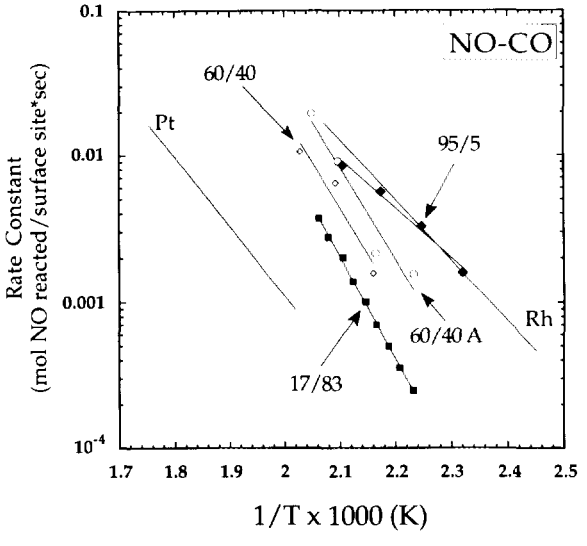

FIG. 6. Plot of log reaction rate constants of the monometallic catalysts, 60/40, 60/40A, 17/83, and 95/5 catalysts versus inverse temperature for the NO–CO reaction. Data points for Pt and Rh are excluded for clarity. Symbols: squares, 17/83; open diamonds, 60/40; open circles, 60/40A; diamonds, 95/5.

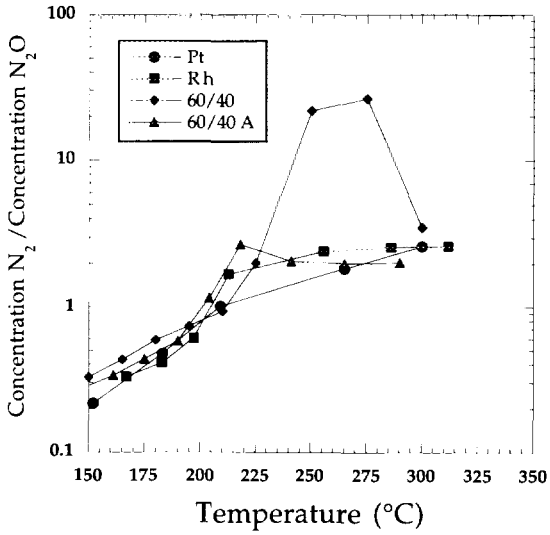

FIG. 7. $NO-H_2$ reaction selectivity plotted as the ratio of N_2 concentration to N_2O concentration versus temperature for the monometallic catalysts, 60/40, and 60/40A catalysts.

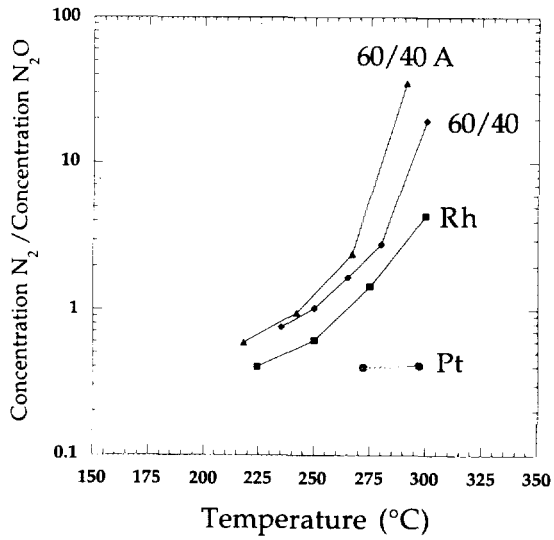

FIG. 9. NO–CO reaction selectivity plotted as the ratio of N_2 concentration to N_2O concentration versus temperature for the monometallic catalysts, 60/40, and 60/40A catalysts. Symbols: diamonds, 60/40; triangles, 60/40A; squares, Rh; circles, Pt.

Reaction Selectivity

The selectivity results for the $NO-H_2$ reaction are presented as the ratio of the concentration of N_2 to the concentration of N_2O. This ratio was observed to increase with increasing temperature for the monometallic catalysts, with N_2 becoming the dominant product at about 210°C (Fig. 7). A maximum in N_2/N_2O selectivity ratio of 30 : 1 was achieved by the 60/40 catalyst at approximately 270°C, while at the same temperature the 60/40A catalyst, and both monometallic catalysts, displayed a nearly equal N_2 selectivity ratio of about 1.5 : 1. The selectivity results for the 95/5 and 17/83 catalysts are presented in Fig. 8. NO reduction selectivity to N_2 for the $NO-H_2$ reaction increased with increasing temperature for both of these catalysts, surpassing the N_2O selectivity at about 210°C. Above 220°C, both the 95/5 and the 17/83 catalysts displayed greater N_2 selectivity than either Pt or Rh monometallic catalysts. The 95/5 catalyst displayed the best selectivity, approaching 100% N_2 selectivity above 270°C.

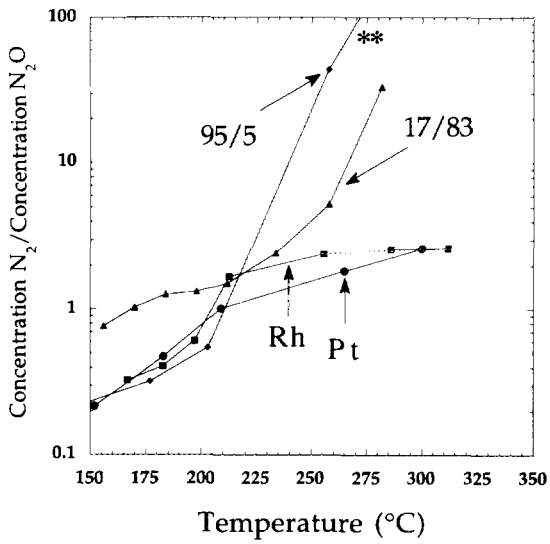

FIG. 8. $NO-H_2$ reaction selectivity plotted as the ratio of N_2 concentration to N_2O concentration versus temperature for the monometallic catalysts, 17/83, and 95/5 catalysts. **Indicates nearly 100% N_2 selectivity. Symbols: diamonds, 95/5; triangles, 17/83; squares, Rh; circles, Pt.

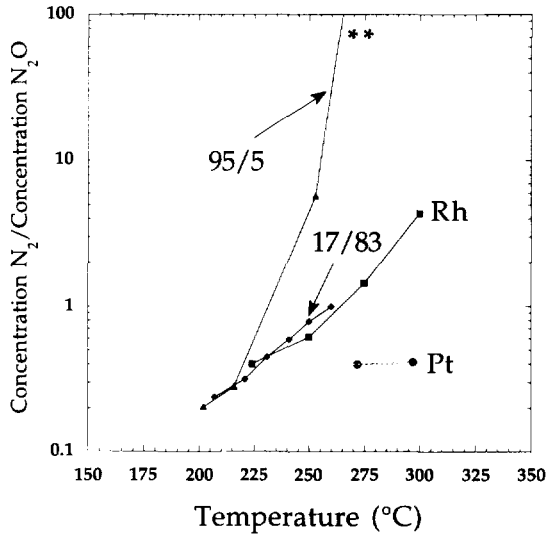

FIG. 10. NO–CO reaction selectivity plotted as the ratio of N_2 concentration to N_2O concentration versus temperature for the monometallic catalysts, 17/83, and 95/5 catalysts. **Indicates nearly 100% N_2 selectivity. Symbols: diamonds, 17/83; triangles, 95/5; squares, Rh; circles, Pt.

The NO–CO reaction selectivity results are presented in Figs. 9 and 10. For this reaction, as was the case for the NO–H_2 reaction, there is a trend toward increased N_2 selectivity with increasing temperature for all of the catalysts. Only two data points are available for the Pt catalyst because of the low conversion observed for Pt below 300°C. The 60/40A catalyst consistently displayed greater N_2 selectivity than the 60/40 and monometallic catalysts (Fig. 9). Figure 10 indicates that the 95/5 catalyst is substantially more selective toward the formation of N_2 than the 17/83 catalyst, and as was the case for the NO–H_2 reaction, the 95/5 catalyst displayed higher N_2 selectivity for the NO–CO reaction than all other catalysts tested.

DISCUSSION

NO Reduction Activity

The data presented in Results of this investigation were given in roughly chronological order. The 60/40 catalysts were a first attempt at forming uniformly alloyed Pt–Rh particles, but after AEM was performed it became obvious that catalysts with less complicated particle composition distributions would be required to relate particle microstructure to performance (6). This realization lead to the preparation of the 95/5 and 17/83 catalysts which were designed to be unimodally dispersed, based upon the validity of applying the Pt–Rh phase diagram to these highly dispersed alloy particles. The 95/5 and 17/83 compositions were selected to lie on the phase boundaries of the miscibility gap in the Pt–Rh alloy phase diagram, which would result in distributions that contained only Pt-rich or Rh-rich particles. The AEM data on these catalysts showed that the preparations were successful in producing well-defined particle composition distributions. The performance of the 95/5 and 17/83 catalysts can therefore be interpreted as the catalytic activity of Pt-rich and Rh-rich alloy particles, respectively. Thus, the discussion of catalytic activity and synergistic activity effects due to particle alloying will begin with these catalysts.

Table 2 contains a summary of the apparent activation energies and pre-exponential factors of the apparent reaction rate constants for both reactions. For the NO–H_2 reaction, the Pt monometallic catalyst was about 1000 times more active than Rh, and the 95/5 catalyst outperformed Pt, while the 17/83 catalyst performed like Rh. If there is a reaction synergism due to Pt–Rh alloying, the performance of the alloy would be greater than the sum of the performance expected from the individual components if they were not alloyed. Unfortunately, no information is available concerning the surface composition of the individual alloy particles, and the possibility of surface segregation of one component cannot be overlooked. If the 95/5 catalyst is considered, there are three possible models for surface segregation:

(1) All of the Rh in the catalyst is present on an active surface due to Rh segregation.

(2) No preferential segregation is occurring, and the particle surface composition reflects the bulk composition of the catalyst.

(3) Pt surface segregates and effectively buries all the Rh.

The calculated surface compositions for each each of these segregation models is presented in Table 3.

If it is assumed that the Pt and Rh atoms in alloyed particles do not interact, the measured reaction rate constants for the monometallic Pt and Rh catalysts can be used to model the performance of the above surface concentration models. For the 95/5 catalyst, the performance anticipated for the Pt segregation and bulk composition models are essentially equal (Fig. 11). If surface segregation of Rh were occurring, the anticipated performance is indicated by the line labeled "Rh Segregation Model." Since the observed reaction-rate constants for 95/5 are greater than those predicted by any model of particle surface segregation, then the enhanced performance of the Pt-rich alloy particles may be considered synergistic.

Similar theoretical surface composition calculations were performed for the 17/83 catalyst. Figure 12 contains the theoretical performance of the surface segregation models assuming Pt and Rh do not interact on the surface of the particles. The performance anticipated for the Pt segregation and bulk composition models nearly overlap. The observed performance of the 17/83 catalyst for the NO–H_2 reaction is only slightly greater than the performance of the Rh surface segregation model. This would suggest, if Pt and Rh are not kinetically interacting, that Rh is segregating to the surface of the Rh-rich particles and no synergistic effect is present.

TABLE 3

Calculated Surface Compositions in Atomic Percentage for Three Surface Segregation Models

	Surface composition in atomic percentage		
Catalyst	Minor component segregates	Major component segregates	Bulk composition
95/5	Rh segregates to surface 70% Pt 30% Rh	Pt segregates to surface 100% Pt	91% Pt 9% Rh
17/83	Pt segregates to surface 12% Pt 88% Rh	Rh segregates to surface 100% Rh	10% Pt 90% Rh

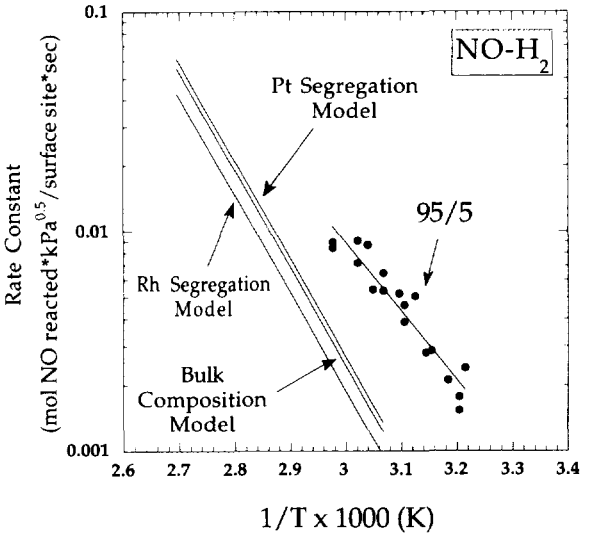

FIG. 11. Replot of reaction rate constant versus inverse temperature for the NO–H_2 reaction over the 95/5 catalyst. The theoretical performance of surface segregation models are also presented.

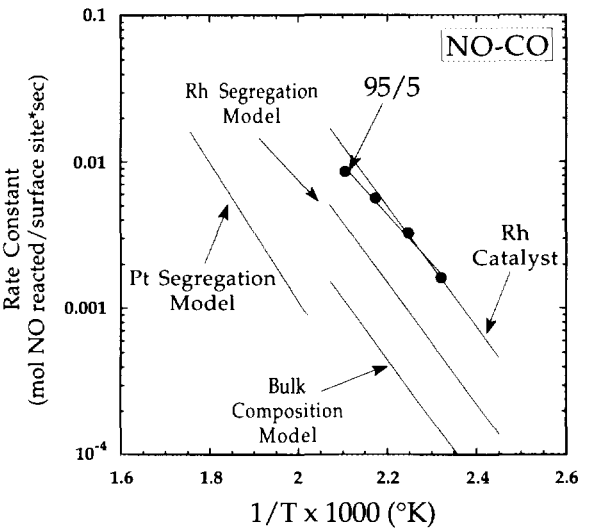

FIG. 13. Replot of reaction rate constant versus inverse temperature for the NO–CO reaction over the 95/5 catalyst. The theoretical performance of surface segregation models are also presented.

The kinetic results of the 95/5 and 17/83 catalysts suggest that for the NO–H_2 reaction, Pt-rich alloy particles display a synergistic activity effect. Rhodium appears to surface segregate in Rh-rich particles and perform like a Rh monometallic catalyst.

With this knowledge, it is possible to interpret the performance of the 60/40 catalysts which are made up of both types of particles. The following discussion pertains to both the 60/40 and the 60/40A catalyst, but the discussion will focus on the 60/40 catalyst. This catalyst contained a bimodal particle composition distribution composed of Pt-rich and Rh rich particles (6). Based on the above discussion, the Rh-rich particles are expected to behave like Rh, and the Pt-rich are expected to perform better than Pt. It is therefore not surprising that the 60/40 catalysts had an intermediate performance between the Pt and Rh monometallic performance.

Similar theoretical calculations were performed for the NO–CO reaction. Figures 13 and 14 contain the theoretical performance of the surface segregation models assum-

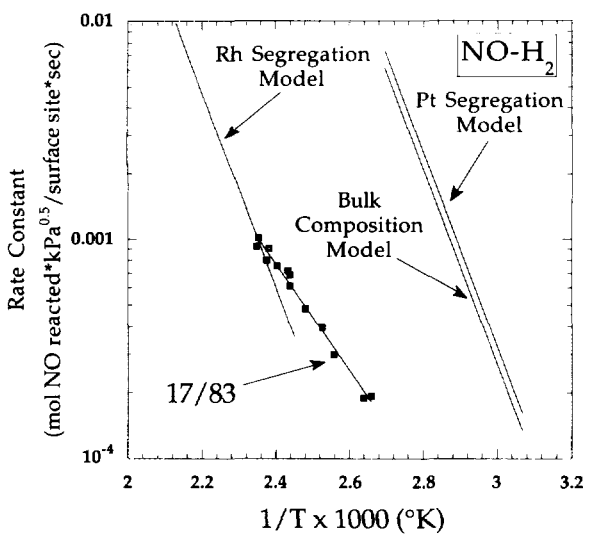

FIG. 12. Replot of reaction rate constant versus inverse temperature for the NO–H_2 reaction over the 17/83 catalyst. The theoretical performance of surface segregation models are also presented.

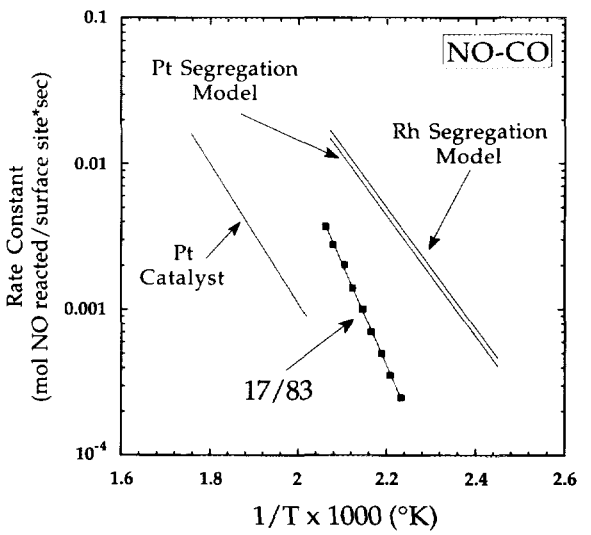

FIG. 14. Replot of reaction rate constant versus inverse temperature for the NO–CO reaction over the 17/83 catalyst. The theoretical performance of surface segregation models are also presented.

ing Pt and Rh do not interact. The performance of the 95/5 catalyst exceeded the predicted performance of any of the surface segregation models. The reaction rates of 95/5 approached those of the Rh monometallic catalyst, which was the most active monometallic catalyst for the NO–CO reaction, even though this catalyst contained the least Rh of any alloy catalyst tested. For the 17/83 catalyst, all of the segregation models predict reaction rate constants very close to those measured for the Rh monometallic catalyst, and are bound by the Pt segregation model and the Rh segregation model. The observed rate constants for the Rh-rich particles of the 17/83 catalysts were less than those predicted by any of the surface composition models. This indicates these Rh-rich alloy particles perform worse than is expected from the sum of the unalloyed components. Further investigations are necessary to address this unexpected result.

The Synergistic Effect

The experimental evidence presented in this study has established the presence of synergistic behavior in Pt-rich, Pt-Rh alloy catalysts for the NO–H_2 and NO–CO reactions at temperatures up to 300°C. A decrease in NO reduction activity for the NO–CO reaction was observed for Rh-rich particles relative to the expected performance of the alloy components. A major weakness in many of the previously published investigations concerning synergistic effects of alloying, is a lack of high spatial resolution chemical analysis (analytical electron microscopy). The synergism observed during this investigation could be easily obscured in some experiments by catalyst materials which possess complex particle composition distributions. This was the case in the first studies performed in this laboratory. The 60/40 catalysts contained both Pt-rich and Rh-rich alloy particles. The reaction kinetics were therefore a mixture of the synergistic alloying effects observed for Pt-rich particles and the nonsynergistic effects observed for Rh-rich particles. The resulting averaged behavior was misleading and suggested the absence of a syngeristic alloying effect. This may explain why Nieuwenhuys group did not observe synergism. Although they used different precursors and support material for their coimpregnation process, it is certainly possible that they may have produced the same bimodal particle compositions, observed for the 60/40 and the 72/28 coimpregnated catalysts, which did not display synergism.

The catalyst prepared by Oh and Carpenter (1), which displayed CO oxidation synergism, was prepared with different precursors, but may be compared to the 75/25 Rh_{ox}–Pt_{red} catalyst prepared for this investigation. Their average particle composition was 68 wt% Pt and by the designation scheme of this study would be 68/32. Their first processing step was Rh impregnation followed by a 300°C calcination, and next Pt was impregnated and calcined at 500°C. Although in the present work, the 75/25 Rh_{ox}–Pt_{red} catalyst was reduced following Pt impregnation, Pt calcination was not observed to inhibit particle alloying in the 60/40 catalysts, or the 95/5 and 17/83 catalysts. Therefore Oh and Carpenter's catalyst preparation procedure should have also produced the Pt-rich particles that were observed in the 75/25 Rh_{ox}–Pt_{red} catalyst. The 75/25 Rh_{ox}–Pt_{red} catalyst and the 95/5 catalyst performed similarly (synergistically) for the NO–H_2 reaction.This study reaches the same conclusion: a reaction synergism is present for a catalyst prepared in this manner.

Oh and Carpenter also made coimpregnated catalysts which were calcined at 500°C, with an average particle composition of 60 wt% Pt, that did not show reaction synergism. Based upon the results of the present investigation, the lack of synergism for this catalyst is not surprising. It is likely that they too formed both Pt-rich and Rh-rich particles by coimpregnation, and the averaged performance of these two types of particles was not synergistic.

This investigation has related the synergistic catalytic effect due to particle alloying with particle composition, however it is unclear what actually causes the improved performance. Recent Monte-Carlo calculations by Herz *et al.* (12) suggest that for a bimolecular surface reaction, a composite material composed of two different types of surface sites, each with optimal properties for the adsorption of one component (each type of site would possess a high surface coverage of one reactant species), would perform better than a single material. This composite structure would eliminate site competition and increase reaction rates by increasing the probability of having both reactive species on neighboring sites.

Herz *et al.* predict a substantial increase in reaction rates for CO oxidation if a catalytic surface is composed of one type of site which adsorbs CO and another type of site which adsorbs O_2 only. This argument implies that the observed improvement in reaction rates is due to structural or geometrical effects. The surface structure of the alloy catalyst which displays synergism is proposed to be a statistical mixture of the two different metal sites whose surface properties are identical to those in the unalloyed state. However, because each type of site selectively adsorbs one reaction component there is an increased probability of having both reaction species in close proximity in the statistical mixture, compared to the same probability over a single type of site which strongly adsorbs one reacting species. A second possibility, is that when the two alloy components are next to each other on a surface they interact electronically. This would alter the surface properties of the metals and create a new type of surface site that could be responsible for improved performance. Mechanistically these two possible effects

are quite different, but from a microstructural point of view they both could arise from the same combination of the two metals on the reactive surface.

During the NO–CO reaction Pt surfaces are known to be dominated by the presence of CO (13, 14). Therefore, the relatively low reaction-rate constants observed for Pt can be explained on the basis of CO site blocking. Conversely, the surfaces of Rh have been shown to be dominated by the presence of NO (15, 17). This would therefore result in relatively higher apparent rate constants for the NO–CO reaction over Rh. Further evidence to support the high surface coverage of NO on Rh is the strong inhibition effect which NO has on the CO oxidation reaction over Rh (18). The relative performance of the Pt and Rh monometallic catalysts can therefore be interpreted on the basis of surface site competition of the reactive species on the single metal catalysts.

On a similar basis consider the 95/5 catalyst. The AEM results indicated that the metal particles of the 95/5 alloy catalyst were Pt-rich. Table 3 contains the possible extremes of surface composition based upon the total metal content of the catalyst. If every atom of Rh in the catalyst were on a surface, the maximum Rh surface composition would be 30 at.%. The minimum possible surface concentration of Rh is 0 at.%, caused by Pt surface segregation. Since the catalyst does not peform like Pt, it is safe to assume that there is a non-zero surface composition of Rh which must be less than 30 at.%. With this assumption, consider the observed synergism of the 95/5 catalyst for the NO–CO reaction. If the surfaces of the alloy particles are viewed as containing islands of Rh among a sea of Pt, then the modeling results of Herz *et al.* (12) may be extended to Pt–Rh alloy catalysts for the NO–CO reaction. The observed increase in reaction rates may be due to the increased probability of finding NO in the vicinity of CO if the Rh islands adsorb mostly NO, and Pt adsorbs mostly CO. The effective boundary area between Pt and Rh islands may be expected to be quite high. At these boundaries the probability of forming the activated NO–CO complex could be much higher than the probability of forming the activated complex on a monometallic surface, where the reactive species are competing for the same adsorption sites. This is especially true for the case when one reactive species is known to dominate the active surface.

Similar arguments for increased apparent reaction rate constants for the NO–H_2 reaction may also be made. For this reaction, the surfaces of Pt are considered to be dominated by the presence of H_2 (24), and Rh strongly adsorbs NO (10, 19). According to the kinetic model, this would predict that Pt is more active than Rh for this reaction, and that is precisely what was observed. The 95/5 catalyst surface may again be considered a mixture of Pt and Rh sites, and equivalently a mixture of surface regions with high NO or high H_2 concentrations. Therefore, the increased reaction probability at the boundary between these sites due to the noncompetitive adsorption of NO and H_2 on neighboring sites increased the observed apparent reaction rate constants. For the NO–H_2 reaction the 17/83 catalyst performed similarly to Rh, and may indicate that for this reaction Rh segregated to the surface of the catalyst and effectively buried the Pt.

NO Reduction Selectivity

N_2O was the primary reaction product produced by the Pt and Rh monometallic catalysts for the NO–H_2 reaction below about 200°C (Figs. 7 and 8). Nitrogen selectivity increased with increasing temperature and plateaued at 250°C with a maximum N_2/N_2O concentration ratio of 3 (Fig. 7). When considering the commercial application of these catalysts, it would be important to minimize the formation of N_2O which contributes to both stratospheric ozone destruction and greenhouse warming (20).

The 60/40 and 60/40A catalysts followed the same basic selectivity trends observed for the monometallic catalysts. A notable exception occurred for the 60/40A catalyst between 250 and 280°C. In this temperature range the observed N_2/N_2O concentration ratio increased from 3 to almost 30. The 95/5 and 17/83 catalysts also displayed greater N_2 selectivity than the monometallic catalysts above 230°C, and in this temperature region the 95/5 provided consistently better N_2 selectivity. The following is a list of the catalysts in order of decreasing N_2 selectivity for the NO–H_2 reaction at 275°C:

$$95/5 > 60/40 > 17/83 > Rh > 60/40A > Pt.$$

The N_2 selectivities for the NO–CO reaction are presented in Figs. 9 and 10. Rh is much more selective for the formation of N_2 than Pt, and all of the alloy catalysts performed at least as well as Rh. The following is a list of the catalysts in order of decreasing N_2 selectivity for the NO–CO reaction at 275°C:

$$95/5 > 60/40A > 60/40 > 17/83 > Rh > Pt.$$

All of the alloy catalysts display greater N_2 selectivity for the NO–CO reaction than the monometallic catalysts. This suggests that there is synergistic selectivity effect due to particle alloying for the NO–CO reaction. The Rh-rich particles of the 17/83 catalyst perform just slightly better than the Rh monometallic catalyst, while the Pt-rich alloy particles of the 95/5 catalyst display the greatest selectivity.

CONCLUSION

1. A synergistic activity effect due to particle alloying is present for Pt-rich alloy particles in the NO–H_2 and

NO–CO reactions. NO–H_2 and NO–CO reaction studies found that catalysts which contained only Pt-rich particles performed significantly better than what is expected from the performance of the alloy components. It is therefore concluded that for the Pt-rich alloy particles, a synergistic effect due to particle alloying is present. For a catalyst which contained primarily Rh-rich alloy particles a detrimental alloying effect on reaction activity was observed for the NO–CO reaction. The reduction activity for this catalyst was less than that expected from the sum of the alloy components. These observations were shown to be easily concealed in the microstructural diversity of catalysts which contained both Pt-rich and Rh-rich particles.

2. A synergistic N_2 selectivity effect due to particle alloying is present for Pt–Rh alloy particles in the NO–H_2 and NO–CO reactions. In all but one case, the alloy catalysts tested displayed N_2 selectivities greater than or equal to the best performing monometallic catalyst.

3. This investigation has highlighted the importance of analytical electron microscopy to the catalyst community. The kinetic conclusions reached in this investigation were made possible by the particle concentration-size distributions presented in the preceding paper. Without the analysis of individual catalyst particles, this investigation would have been unable to associate reaction synergism with the Pt-rich alloy particles.

ACKNOWLEDGMENTS

The authors acknowledge Michael Saeger and Joseph Herman for their assistance in providing the kinetic measurements presented in this investigation. The authors also gratefully acknowledge the financial support of the U.S. Department of Energy under contract DE-FG02-86ER45269.

REFERENCES

1. Oh, S. H., and Carpenter, J. E., *J. Catal.* **98,** 178 (1986).
2. D'Aniello, M. J., Jr., U.S. patent 4,380,510, April 19, 1983.
3. Tzou, M. S., Asakura, K., Yamazaki, Y. and Kuroda, H., *Catal. Lett.* **11,** 33 (1991).
4. Heezen, L., Kilian, V. N., van Slooten, R. F., Wolf, R. M. and Nieuwenhuys, B. E., *Catal. Automotive Pollut. Control II* **71,** 381 (1991).
5. Van den Bosch-Driebergen, A. G., Kieboom, M. N. H., van Dreumel, A., Wolf, R. M., van Delft, F. C. M. J. M., and Nieuwenhuys, B. E., *Catal. Lett.* **2,** 73 (1989).
6. Lakis, R. E., Lyman, C. E., Stenger, H. G., *J. Catal.* **154,** 261–275 (1995).
7. Anderson, J. A., *J. Catal.* **142,** 153 (1993).
8. Satterfield, C. N., "Heterogeneous Catalysis in Industrial Practice", 2nd ed., p. 127. McGraw-Hill, New York, 1991.
9. Stenger, H. G., and Hepburn, J. S., J. *Energy Fuels* **1,** 412 (1987).
10. Hecker, W. C., Bell, A. T., *J. Catal.* **92,** 247 (1985).
11. Scharpf, E. W., and Benziger, J. B., *J. Catal.* **136,** 342 (1992).
12. Herz, R. K., Badlani, A., Schryer, D. R., Upchurch, B. T. J. T., *J. Catal.* **141,** 219 (1993).
13. Lorimer, D., Bell, A. T., *J. Catal.* **59,** 223 (1979).
14. Brown, M. F., Gonzalez, R. D., *J. Catal.* **44,** 477 (1976).
15. Hecker, W. C., Bell, A. T., *J. Catal.* **84,** 200 (1984).
16. Arai, H., Tominaga, H., *J. Catal.* **43,** 131 (1976).
17. Solymosi, F., Sarkany, J., *Appl. Surf. Sci.* **3,** 68 (1979).
18. Oh, S. H. and Carpenter, J. E., *J. Catal.* **101,** 114 (1986).
19. Savatsky, B. L., Bell, A. T., *ACS Symp. Ser.* **178,** 105 (1982).
20. Armor, J. N., *Appl. Catal. B* **1,** 221 (1992).
21. Klein, R. L., Schwartz, S., Schmidt, L. D., *J. Phys. Chem.* **89,** 4908 (1985).
22. Hendershot, R. E., Hansen, R. S., *J. Catal.* **98,** 150 (1986).
23. Hecker, W. C., Bell, A. T., *J. Catal.* **84,** 200 (1983).
24. Papapolymerou, G. A., Schmidt, L. D., *Langmuir* **1,** 488 (1985).